

# Mapping PASL Arterial Transit Time in Normal Human Brain using [15O]water PET

M. Qiu<sup>1</sup>, J. Wang<sup>1</sup>, H. Kim<sup>1</sup>, R. E. Carson<sup>1</sup>, and R. T. Constable<sup>1</sup>

<sup>1</sup>Yale University School of Medicine, New Haven, CT, United States

**Introduction** Arterial transit time (ATT) in pulsed arterial spin labeling (PASL) refers to the time it takes the arterial blood to travel from the labeling site to the capillaries. It defines the earliest time data acquisition could start after IR labeling and is required for CBF quantification. Two approaches have been used to address the ATT uncertainty: first, ATT values are measured using the PASL sequence with images collected at different post-labeling delay times, TI [1]; second, ATT is assumed to be linearly related to TI as in QUIPPS II, where  $\tau_a = TI - TI_1$ ,  $T_{I_1} = 700$  ms. ATT measurements that use the PASL sequence suffer from the low sensitivity of PASL and intravascular contamination. In both cases, ATT is determined on a per-slice basis and within slice variations in ATT are not considered. The use of improper ATT values can introduce errors in CBF quantification. In this study we used CBF measured by PET to calculate the ATT on a per-voxel basis, which allows us not only to examine the in-slice ATT variability, but also to optimize the ATT values assigned to slices. More important, the ATT map, once estimated, can be used for CBF mapping in a similar PASL imaging setup, providing voxel based ATT values.

**Methods and Materials** Thirteen consenting healthy subjects (males,  $27 \pm 6$  years) were recruited. Both PASL and PET images were collected on each subject, during 2 visits scheduled on different days, once for MRI, once for PET. MRI was performed on a 3T whole-body scanner Trio (Siemens Medical Systems, Erlangen, Germany) with a CP head coil. EPSTAR QUIPSS ASL MRI [2] was used to measure CBF and total 270 PASL images were collected for the resting state during the MR scan. The acquisition parameters were: FOV = 240x264 mm<sup>2</sup>; matrix = 60x64; bandwidth = 2442 Hz/pixel; slice thickness = 6 mm (gap 3 mm). Ten AC-PC aligned slices were acquired from inferior to superior in an ascending order with the lowest slice passing through AC-PC. Between the imaging and labeling slabs there was a 20-mm gap. Acquisition of each slice took approximately 60 ms. TI = 1400 ms; TR = 2000 ms; TE = 21 ms;  $T_{I_a} = 1490$  ms;  $\lambda = 0.9$  ml/g, and  $\alpha_\pi = 0.95$ . Proton density-weighted image ( $M_0$ ) was acquired by the same PASL sequence except TR = 10000 ms and TI = 9000 ms. The  $T_{I_{app}}$  map was measured by an ultrafast Look-Locker echo-planar imaging sequence [3]. PET imaging was performed using High Resolution Research Tomograph (HRRT) which acquires 207 slices (1.2 mm slice separation) with reconstructed image resolution of  $\sim 3$  mm. A 6-min transmission scan was acquired for attenuation correction. Twelve bolus injections (20-s duration) of 20 mCi of [<sup>15</sup>O]water each were administered through an intravenous line at intervals of 10 mins using an infusion pump. List mode data were acquired on the HRRT for each scan. Acquisition of HRRT list mode data began shortly before each injection. Simultaneously, the arterial input function was measured with an automated blood counting system (PBS-101, Veenstra Instruments) using continuous withdrawal system with a peristaltic pump (4 ml/min). The radioactivity in whole blood was measured with a calibrated radioactivity monitor. The total blood withdrawal per injection was < 20 ml. During the 12 [<sup>15</sup>O]water scans. The task acquisition (performed in random order) consists of: Four baseline [<sup>15</sup>O]water scans were performed on each subject, each for  $\sim 5$  min.

**Data processing and ATT mapping** Images of intensity changes ( $\Delta M$ ) were calculated by simply averaging all the PASL “label-control” differences. The  $M_0$ ,  $T_{I_{app}}$ ,  $\Delta M$  images and the CBF data measured by PET ( $f_{PET}$ ) were all transformed to a standard whole brain template space (NMI, 3x3x3 mm<sup>3</sup>, matrix 58x72x52). To register the slice information in the common space, for each individual PASL dataset, we created a 3D image and assigned a number (1 to 10) to each slice indicating the acquisition order. This 3D image has the same geometric information as  $M_0$  and it was transformed to the common space using the same transformations as applied to  $M_0$ . These transformed images provide information on when a voxel was acquired, and the TI associated with any voxel is easily determined. By rearranging the terms of the equation used for CBF calculation in PASL [4], the following equations for the ATT ( $\tau_a$ ) mapping in this study are obtained:

$$\tau_a = TI - \frac{\lambda \Delta M(TI) e^{TI/T_{I_a}}}{2c f_{PET} M_0} \quad (1)$$

$$c = \alpha_\pi \frac{1 - e^{-(TI - \tau_a)(1/T_{I_{app}} - 1/T_{I_a})}}{(TI - \tau_a)(1/T_{I_{app}} - 1/T_{I_a})} \quad (2)$$

**Results and discussion** The individual ATT maps were calculated using Equations (1) and (2). The mean ATT map in the common space is shown in Fig 1. The ATT value and the spatial standard deviation of ATT were measured for each slice. These data were then pooled across subjects and shown in Fig 2. The spatial standard deviation within each of the slices is displayed as yellow bars, showing marked spatial variability in the ATT within slices. Slices from the lower part of the brain exhibit more spatial variability. Single mean ATT values assigned to the slices will lead to overestimation of CBF in regions with small ATT values and underestimation of CBF in regions with large ATT's. The ATT increases linearly in slices acquired in ascending order (red bars), with the green line providing the best fit to the data in Fig 2. The fit indicates an optimal TI 6% greater than the TI used to acquire the PASL data and an optimal  $T_{I_1}$  of 875 ms. Using QUIPSS II with  $\tau_a = TI - 700$  ms, CBF would be underestimated.

**Conclusion** In this study we demonstrated that errors in CBF are generated when in-slice ATT variability is ignored and demonstrate the advantage of using a voxel-based measure of ATT. This approach provides guidance for optimizing PASL parameters. Furthermore, the ATT map generated, can be used for input into quantitative calculations of regional CBF.

**References:** [1] Yang et. al. 2000. MRM 44:680-5; [2] Luh WM et. al. 1999. MRM41(6);1246-54; [3] Freeman AJ et. al. 1998. MRI 16(7):765-72; [4] Yang et. al. 1998. MRM 39:825-32.

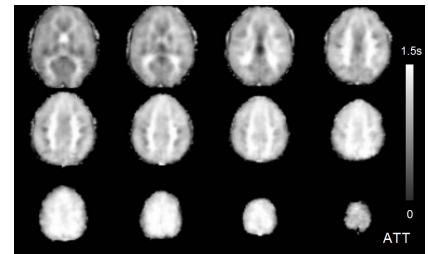


Fig 1 Slices of ATT in the common space.

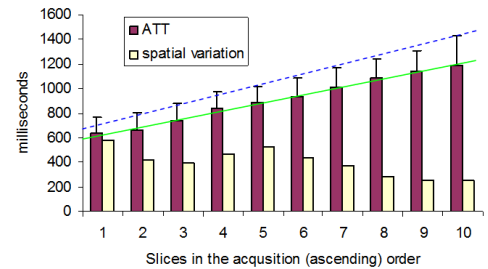


Fig 2 ATT was calculated on a per-slice basis (red bars), with in-slice variability (yellow bars). The error bars show the standard deviation of these ATT measurements on the subject-pooled data. Blue dashed line:  $\tau_a = TI - 700$  ms; Green solid:  $\tau_a = 1.06 TI - 875$ .